VNU Journal of Science: Mathematics - Physics

Journal homepage: https://js.vnu.edu.vn/MaP

Original Article

Nonlinear Vibration of Function Graded Magneto-electro-elastic Microplates using Nonlocal Stress Theory

Ngo Dinh Dat*, Nguyen Dinh Duc

VNU University of Engineering and Technology, 144 Xuan Thuy, Cau Giay, Hanoi, Vietnam

Received 19 June 2023
Revised 28 June 2023; Accepted 03 July 2023

Abstract: This work presents an analysis of nonlinear vibration in Function Graded Magneto-Electro-Elastic (FG-MEE) plates subjected to mechanical, electrical, and magnetic loads using the nonlocal stress theory approach. In this study two types of MEE plates, namely $BaTiO_3$ and $CoFe_2O_4$ were considered. The basic equations are derived using classical plate theory with nonlocal stress theory and are solved using the Galerkin method and Runge-Kutta method. We investigated the effects of nonlocal parameters, materials, and geometrical characteristics on the natural frequencies and nonlinear vibration of the FG-MEE microplates.

Keywords: FGM; MEE; Vibration; Nonlocal stress theory.

1. Introduction

Functionally graded materials offer several advantages in terms of their resistance to the coupling of various conditions, where material discontinuity can significantly affect the performance of structural systems. A new class of adaptive structures or smart composites has emerged, consisting of both piezoelectric and electromagnetic materials. These structures and composites are commonly known as multilayer composites or magneto-electro-elastic (MEE) composites. They have shown promising potential in a wide range of applications, including microelectromechanical systems (MEMS) and nanoelectromechanical systems (NEMS), sensors, actuators, and wireless communication devices [1]. Zhou et al., utilized a smoothed cell-based finite element method for static and dynamic analyses of magneto-electro-elastic structures under uniformly increasing temperature [2-3]. Hsu and Hwu [4]

* Corresponding author.
E-mail address: ngodinhdat0405@gmail.com

https//doi.org/10.25073/2588-1124/vnumap.4858

analyzed the elongation-bending boundary element for asymmetric magneto-electro-elastic plates with multiple holes, cracks, and impurities based on the corresponding boundary element method for coupled stretching-bending composite plates. Kuo and Wang [5] used the pseudo-Stroh formulation and propagation matrix method to calculate wave motion analysis solutions for layered magneto-electro-elastic plates with interface defects of membrane type. Zhang et al., [6] addressed issues of nonlinear oscillation and bending of multilayer magneto-electric beams in thermal environment based on high-order shear deformation theory combined with the von-Karman nonlinear dynamic model. Vinyas et al., [7] examined the impact of varying the thickness of the alternating current on the frequency of three-phase smart magneto-electro-elastic plates. Furthermore, Zhou et al., [8] investigated the dynamic characteristics of smart composite structures under combined thermal loads and mechanical loads. Chen et al., [9] proposed a vector state method to study the free vibration of magneto-electro-elastic laminated plates. Dat et al., [10-11] analyzed the nonlinear magneto-electro-elastic vibration of a smart sandwich plate placed on a Pasternak-type elastic foundation and subjected to combined external pressure, thermal, electric, and magnetic loads.

Non-classical continuum theories are used to analyze the properties of materials at the nanoscale or to study the behavior of materials with complex structures such as composite materials, biological tissues, and porous materials. These theories are also useful in the design and analysis of advanced materials used in aerospace, automotive, and biomedical applications. Liu et al., [12] based on the Almansi theory and the Schmidt method presented a non-local theoretical solution for three-dimensional rectangular penetrating cracks in electroelastic materials. Zhang et al., [13] investigated the effects of surface and nonlocal elasticity on the dispersion relationship of piezoelectric nanosheets. Meanwhile, Chen et al., [14] studied the relationship between the nonlocal parameter and the reflectance and transmission coefficients of planar waves for liquid-submerged multilayer MEE plates.

After conducting a careful investigation of the available literature, it has been observed that most of the studies related to the nonlocal stress theory focus on plates. It can be concluded that despite the high demand for understanding, no research has been conducted on microplates with function graded magneto-electro-elastic using the nonlocal stress theory approach. Therefore, the aim of this work is to investigate the effect of nonlocal parameters, material properties, mechanical, electrical, and magnetic loads on the nonlinear vibration of the microplate.

2. Analytical Solution

2.1. Modeling of Structure

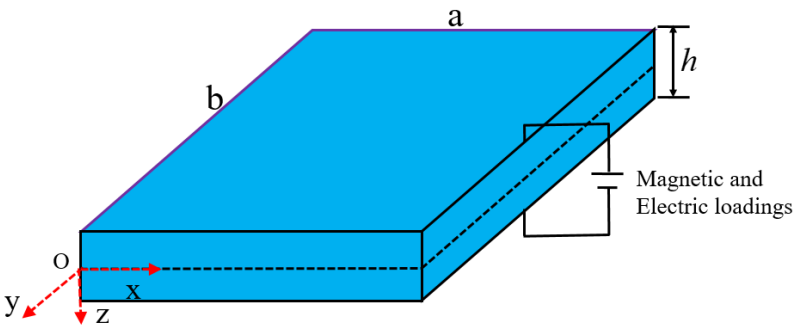

Figure 1. The model of magneto-electro-elastic microplate.

Consider a rectangular Magneto-electro-elastic plate as shown in Fig. 1. This figure shows an MEE microplate with dimensions of length (a), width (b), and thickness (h). The plate is attached to a Cartesian coordinate system (x, y, z), where the z-axis is aligned with the thickness of the plate, and the x-y plane is located on the neutral plane of the microplate.

2.2. Theory and Formulations

The nonlocal stress theory for FG-MEE microplate

The equation representing the constitutive relationship for the nonlocal stress tensor is as follows: [15]:

$$\sigma = \int_v K\left(\left|X' - X\right|, \tau\right) t\left(x'\right) dx', \tag{1}$$

in which σ, σ' are local and nonlocal stress tensors module $K\left(\left|X' - X\right|, \tau\right)$ represents the interaction between two points of the material X and X'; $\tau = e_0 a / l, e_0$ is a constant appreciation to the material; a and l are the internal and external length, respectively.

The more commonly used differential form [15] of the nonlocal constitutive relation is shown below: $\sigma - \eta\nabla^2\sigma = \sigma'$ in which $\eta = \left(e_0 a\right)^2$ specifies the nonlocal parameter and $\nabla^2 = \partial_{,x^2} + \partial_{,y^2}$ is the Laplacian operator.

Basic equations

Based on the classical plate theory, the relationships between strain and displacement have been established as follows:

$$\begin{bmatrix} \varepsilon_x \\ \varepsilon_y \\ \gamma_{xy} \end{bmatrix} = \begin{bmatrix} \varepsilon_x^0 \\ \varepsilon_y^0 \\ \gamma_{xy}^0 \end{bmatrix} + z \begin{bmatrix} k_x \\ k_y \\ 2k_{xy} \end{bmatrix} = \begin{bmatrix} u_{,x} + 0.5\left(w_{,x}\right)^2 \\ v_{,y} + 0.5\left(w_{,y}\right)^2 \\ u_{,y} + v_{,x} + w_{,x}w_{,y} \end{bmatrix} + z \begin{bmatrix} -w_{,xx} \\ -w_{,yy} \\ -w_{,xy} \end{bmatrix} \tag{2}$$

The stress-strain relations presented in this study take into account the effects of electric and magnetic fields:

$$\begin{aligned}
&\sigma_x^f - \mu^2\nabla^2\sigma_x^f = \overline{C_{11}}\varepsilon_x^0 + \overline{C_{12}}\varepsilon_y^0 - \overline{e_{31}}E_z - \overline{q_{31}}H_z \\
&\sigma_y^f - \mu^2\nabla^2\sigma_y^f = \overline{C_{12}}\varepsilon_x^0 + \overline{C_{22}}\varepsilon_y^0 - \overline{e_{32}}E_z - \overline{q_{32}}H_z, \\
&\sigma_{xy}^f - \mu^2\nabla^2\sigma_{xy}^f = \overline{C_{66}}\gamma_{xy}^0, \\
&D_x^f - \mu^2\nabla^2 D_x^f = \overline{\eta_{11}}E_x + \overline{m_{11}}H_x \\
&D_y^f - \mu^2\nabla^2 D_y^f = \overline{\eta_{22}}E_y + \overline{m_{22}}H_y \\
&D_z^f - \mu^2\nabla^2 D_z^f = \overline{e_{31}}\varepsilon_x + \overline{e_{32}}\varepsilon_y + \overline{\eta_{33}}E_z + \overline{m_{33}}H_z \\
&B_x^f - \mu^2\nabla^2 B_x^f = \overline{m_{11}}E_x + \overline{\mu_{11}}H_x \\
&B_y^f - \mu^2\nabla^2 B_y^f = \overline{m_{22}}E_y + \overline{\mu_{22}}H_y \\
&B_z^f - \mu^2\nabla^2 B_z^f = \overline{q_{31}}\varepsilon_x + \overline{q_{32}}\varepsilon_y + \overline{m_{33}}E_z + \overline{\mu_{33}}H_z
\end{aligned} \tag{3}$$

in which

$$\begin{aligned}
&\overline{C_{11}} = C_{11}^f - \left(C_{13}^f\right)^2 / C_{33}^f, \overline{C_{12}} = C_{12}^f - C_{13}^f C_{23}^f / C_{33}^f, \overline{C_{22}} = C_{22}^f - \left(C_{23}^f\right)^2 / C_{33}^f, \overline{C_{66}} = C_{66}^f, \overline{m_{11}} = m_{11}^f, \\
&\overline{e_{31}} = e_{31}^f - C_{13}^f e_{33}^f / C_{33}^f, \overline{e_{32}} = e_{32}^f - C_{23}^f e_{33}^f / C_{33}^f, \overline{e_{15}} = e_{15}^f, \overline{e_{24}} = e_{24}^f, \overline{q_{31}} = q_{31}^f - C_{13}^f q_{33}^f / C_{33}^f, \overline{\eta_{22}} = \eta_{22}^f, \\
&\overline{q_{32}} = q_{32}^f - C_{23}^f q_{33}^f / C_{33}^f, \overline{b_{11}} = \mu_{11}^f, \overline{b_{22}} = \mu_{22}^f, \overline{b_{33}} = \mu_{33}^f + \left(q_{33}^f\right)^2 / C_{33}^f, \overline{\eta_{11}} = \eta_{11}^f, \\
&\overline{\eta_{33}} = \eta_{33}^f + \left(e_{33}^f\right)^2 / C_{33}^f, \overline{m_{22}} = m_{22}^f, \overline{m_{33}} = m_{33}^f + e_{33}^f q_{33}^f / C_{33}^f,
\end{aligned} \tag{4}$$

The electric and magnetic field components can be expressed in terms of the gradients of the scalar electric and magnetic potentials, denoted as Φ and Ψ, respectively [11]

$$\left\{E_k, H_k\right\} = \left\{-\Phi_{,k}, -\Psi_{,k}\right\}, k = x, y, z. \tag{5}$$

with

$$\begin{aligned}
\Phi(x, \mathrm{y}, z, t) &= -\cos(\beta z)\Phi(x, \mathrm{y}, t) + 2z\phi_0 / h \\
\Psi(x, \mathrm{y}, z, t) &= -\cos(\beta z)\Psi(x, \mathrm{y}, t) + 2z\psi_0 / h
\end{aligned} \tag{6}$$

where $\beta = \pi / h$, $\Phi(x,t), \Psi(x,t)$ are the spatial variation of the electric and magnetic potentials, respectively. Also, ϕ_0 and ψ_0 represent the external electric and magnetic potentials at the initial stage, respectively.

Replacing Eq. (5) into Eq. (6) yields

$$\begin{aligned}
&E_k = \cos(\beta z)\left(\Phi_{,k}\right),\ H_k = \cos(\beta z)\left(\Psi_{,k}\right), k = x, y \\
&E_z = -\beta \sin(\beta z)\Phi - 2\phi_0 / h_f, H_z = -\beta \sin(\beta z)\Psi - 2\psi_0 / h_f.
\end{aligned} \tag{7}$$

The force and moment resultants of the FG-MEE microplate can be expressed by calculating the stress, strain, and displacement components as follows:

$$\left(N_k, M_k\right) = \int_{-h_2/2}^{-h_2/2} \sigma_k^f (1, z)\, dz, \ \ (k = x, y, xy) \tag{8}$$

Introducing Eq. (2) into Eqs. (3), and subsequently substituting the obtained results into Eq. (8), one can obtain follows:

$$\begin{aligned}
N_x &= I_{11}\varepsilon_x^0 + I_{12}\varepsilon_y^0 + L_{11}k_x + L_{12}k_y - I_{13}E_z - L_{13}H_z, \\
N_y &= I_{12}\varepsilon_x^0 + I_{22}\varepsilon_y^0 + L_{12}k_x + L_{22}k_y - I_{14}E_z - L_{14}H_z, \\
N_{xy} &= I_{66}\gamma_{xy}^0 + L_{66}k_{xy}, \\
M_x &= L_{11}\varepsilon_x^0 + L_{12}\varepsilon_y^0 + K_{11}k_x + K_{12}k_y - I_{23}E_z - L_{23}H_z, \\
M_y &= L_{12}\varepsilon_x^0 + L_{22}\varepsilon_y^0 + K_{12}k_x + K_{22}k_y - I_{24}E_z - L_{24}H_z, \\
M_{xy} &= L_{66}\gamma_{xy}^0 + K_{66}k_{xy},
\end{aligned} \tag{9}$$

in which the detail of coefficients $B_{ij}\left(i = \overline{1,2}; j = \overline{1,4}\right)$, B_{66} $(B = I, L), K_{ij}\left(ij = 11,12,22,66\right)$ may be found in Appendix.

The nonlinear motion equations of the microplate are defined as

$$N_{x,x} + N_{xy,y} = 0, \tag{10a}$$

$$N_{xy,x} + N_{y,y} = 0, \tag{10b}$$

$$\left(1-\mu^2\nabla^2\right)\begin{bmatrix} M_{x,x^2} + 2M_{xy,xy} + M_{y,y^2} + N_x \mathrm{w}_{,x^2} + 2N_{xy}\mathrm{w}_{,xy} \\ +N_y \mathrm{w}_{,y^2} + q - k_1 w + k_2\left(\mathrm{w}_{,x^2} + \mathrm{w}_{,y^2}\right) \end{bmatrix} = \rho_1 w_{,tt}. \tag{10c}$$

$$\int_{\frac{-h}{2}}^{\frac{h}{2}} \left(\frac{\partial D_x}{\partial x}\cos(\beta z) + \frac{\partial D_y}{\partial y}\cos(\beta z) + D_z \beta \sin(\beta z) \right) dz = 0 \tag{10d}$$

$$\int_{\frac{-h}{2}}^{\frac{h}{2}} \left(\frac{\partial B_x}{\partial x}\cos(\beta z) + \frac{\partial B_y}{\partial y}\cos(\beta z) + B_z \beta \sin(\beta z) \right) dz = 0 \tag{10e}$$

in which, $q(Pa)$ is an distributed load of the FG-MEE microplate and

$$\rho_1 = \int_{-hc/2}^{hc/2} \rho\ (z) dz \tag{11}$$

To express the deformation compatibility equation for a microplate, we can write

$$\frac{\partial^2 \varepsilon_x^0}{\partial y^2} + \frac{\partial^2 \varepsilon_y^0}{\partial x^2} - \frac{\partial^2 \gamma_{xy}^0}{\partial x \partial y} = \left(\frac{\partial^2 w}{\partial x \partial y} \right)^2 - \frac{\partial^2 w}{\partial x^2}\frac{\partial^2 w}{\partial y^2} \tag{12}$$

Upon introducing this stress function into Eqs. (10) and (12) and carrying out the required transformations, it becomes evident that the resulting six equations can be reduced to two nonlinear equations expressed in terms of the variables w, f, Φ and Ψ. These equations are utilized to investigate the nonlinear vibration of the MEE microplate.

Solution of problem

In this work, four edges of the plate are considered to be simply supported and immovable, and the specific boundary conditions are determined based on the in-plane restraint at the edges. The corresponding boundary conditions are as follows:

$$\begin{aligned} &w = u = M_x = 0, N_x = N_{x0}, x = 0, a \\ &w = v = M_y = 0, N_y = N_{y0}, y = 0, b \end{aligned} \tag{13}$$

with N_{x0}, N_{y0} are pre-buckling compressive force resultant in direction x.

In this approach, the stress function Airy is selected and shown as:

$$N_{xx} = \frac{\partial^2 \wp}{\partial y^2}, N_{yy} = \frac{\partial^2 \wp}{\partial x^2}, N_{xy} = -\frac{\partial^2 \wp}{\partial x \partial y}. \tag{14}$$

To solve four newly obtained equations, while taking into account the boundary conditions (13), we make the following assumptions regarding the approximate solutions:

$$\begin{aligned} &\Psi(x,y,t) = \psi(t)\sin\lambda_m x \sin\delta_n y, \\ &\wp(x,y,t) = T_1\cos 2\lambda_m x + T_2\cos 2\delta_n y + T_3 \sin\lambda_m x \sin\delta_n y + 0.5N_{x0}y^2 + 0.5N_{y0}x^2 \end{aligned} \tag{15}$$

$$w(x,y,t)=W(t)\sin\lambda_m x\sin\delta_n y,\Phi(x,y,t)=\phi(t)\sin\lambda_m x\sin\delta_n y,$$

where $\lambda_m=m\pi/a$, $\delta_n=n\pi/b$, m,n are odd natural numbers and $W(t),\phi(t),\psi(t)$ are time-dependent functions. The coefficients $T_k\,(k=1,2,3)$ are determined by introducing of Eq. (15) into Eq. (12), and:

$$T_1=Y_1W(W+2\mu h),\ T_2=Y_2W(W+2\mu h),\ T_3=Y_3W$$

$$T_1=\frac{\delta_n^2}{32I_{11}^*\lambda_m^2\left(4\eta\lambda_m^2+1\right)},\ T_2=\frac{\lambda_m^2}{32I_{22}^*\delta_n^2\left(4\eta\delta_n^2+1\right)},$$

$$T_3=\frac{-W\left[\left(L_{11}^*+L_{22}^*-2L_{66}\right)\lambda_m^2\delta_n^2+L_{12}^*\delta_n^4+L_{21}^*\lambda_m^4\right]}{\left(I_{11}^*+I_{22}^*\right)\eta\lambda_m^6+\left[\left(I_{11}^*-2I_{12}^*+I_{66}^*\right)\eta\lambda_m^2+\left(I_{22}^*+I_{66}^*-2I_{12}^*\right)\eta\delta_n^2+\left(I_{66}^*-2I_{12}^*\right)\right]\lambda_m^2\delta_n^2+I_{11}^*\lambda_m^4+I_{22}^*\delta_n^4} \tag{16}$$

By substituting the assumed approximate solutions (15) into Eqs. (10) and applying the Galerkin method to the resulting equation yields:

$$y_{11}W+y_{12}W(W+\mu h)+y_{13}W(W+2\mu h)+y_{14}W(W+\mu h)(W+2\mu h)$$

$$y_{15}\phi+y_{16}\psi-\left(N_{x0}\lambda_m^2+N_{y0}\delta_m^2\right)(W+\mu h)+\frac{16}{mn\pi^2}p=\rho_1W_{,tt}$$

$$y_{41}\mathrm{W}+\mathrm{y}_{42}\phi+y_{43}\psi=0$$

$$y_{51}\mathrm{W}+y_{43}\phi+y_{52}\psi=0 \tag{17}$$

where $y_{ij}\,(i=1,\ j=1\div4)$ are shown in Appendix.

The conditions that ensure immovability on all four edges (fixed boundary conditions are satisfied on both the x and y axes), such that

$$\int_0^b\int_0^a\frac{\partial u}{\partial x}dxdy=0,\int_0^a\int_0^b\frac{\partial v}{\partial x}dydx=0. \tag{18}$$

From Eq. (9), we can determine the strain components in the middle surface of the microplate as follows:

$$\varepsilon_x^0=I_{22}^*\left(\frac{\partial^2\wp}{\partial y^2}-\eta\left(\frac{\partial^4\wp}{\partial y^4}+\frac{\partial^4\wp}{\partial x^2\partial y^2}\right)\right)-I_{12}^*\left(\frac{\partial^2\wp}{\partial x^2}-\eta\left(\frac{\partial^4\wp}{\partial x^4}+\frac{\partial^4\wp}{\partial x^2\partial y^2}\right)\right)$$

$$+L_{11}^*\frac{\partial^2w}{\partial x^2}+L_{12}^*\frac{\partial^2w}{\partial y^2}+I_{13}^*\phi_0+L_{13}^*\psi_0,$$

$$\varepsilon_y^0=I_{11}^*\left(\frac{\partial^2\wp}{\partial x^2}-\eta\left(\frac{\partial^4\wp}{\partial x^4}+\frac{\partial^4\wp}{\partial x^2\partial y^2}\right)\right)-I_{12}^*\left(\frac{\partial^2\wp}{\partial y^2}-\eta\left(\frac{\partial^4\wp}{\partial y^4}+\frac{\partial^4\wp}{\partial x^2\partial y^2}\right)\right) \tag{19}$$

$$+L_{21}^*\frac{\partial^2w}{\partial x^2}+L_{22}^*\frac{\partial^2w}{\partial y^2}+I_{14}^*\phi_0+L_{14}^*\psi_0,$$

$$\gamma_{xy}^0=-I_{66}^*\frac{\partial^2\wp}{\partial x\partial y}+I_{66}^*\left(\eta\frac{\partial^3\wp}{\partial x^2\partial y}+\eta\frac{\partial^3\wp}{\partial x\partial y^2}\right)+2L_{66}^*\left(\frac{\partial^2w}{\partial x\partial y}\right)$$

with:

$$
\begin{aligned}
&I_{11}^{*}=\frac{I_{11}}{\Delta}, I_{22}^{*}=\frac{I_{22}}{\Delta}, I_{12}^{*}=\frac{I_{12}}{\Delta}, \Delta=I_{11} I_{22}-I_{12}^{2}, I_{66}^{*}=\frac{1}{I_{66}}, L_{66}^{*}=\frac{L_{66}}{I_{66}}, \\
&I_{11}^{*}=I_{22}^{*} L_{11}-L_{12}^{*} L_{12}, L_{22}^{*}=I_{11}^{*} L_{22}-I_{12}^{*} L_{12}, L_{12}^{*}=I_{22}^{*} L_{12}-I_{12}^{*} L_{22}, \\
&L_{21}^{*}=I_{11}^{*} L_{12}-I_{12}^{*} L_{11}, I_{13}^{*}=\frac{-2}{h_f}\left(I_{22}^{*} I_{13}-I_{12}^{*} I_{14}\right), L_{13}^{*}=\frac{-2}{h_f}\left(I_{22}^{*} L_{13}-I_{12}^{*} L_{14}\right), \\
&I_{14}^{*}=\frac{-2}{h_f}\left(I_{11}^{*} I_{14}-I_{12}^{*} I_{13},\right) L_{14}^{*}=\frac{-2}{h_f}\left(I_{11}^{*} L_{14}-I_{12}^{*} L_{13}\right),
\end{aligned}
\tag{20}
$$

From Eqs. (6) and (19), the derivative of displacements can be determined as

$$
\begin{aligned}
&\frac{\partial v}{\partial y}=I_{11}^{*} \frac{\partial^{2} \wp}{\partial x^{2}}-I_{12}^{*} \frac{\partial^{2} \wp}{\partial y^{2}}+L_{21}^{*} \frac{\partial^{2} w}{\partial x^{2}}+L_{22}^{*} \frac{\partial^{2} w}{\partial y^{2}}+I_{14}^{*} \phi_{0}+L_{14}^{*} \psi_{0}-\frac{1}{2}\left(\frac{\partial w}{\partial y}\right)^{2}. \\
&\frac{\partial u}{\partial x}=I_{22}^{*} \frac{\partial^{2} \wp}{\partial y^{2}}-I_{12}^{*} \frac{\partial^{2} \wp}{\partial x^{2}}+L_{11}^{*} \frac{\partial^{2} w}{\partial x^{2}}+L_{12}^{*} \frac{\partial^{2} w}{\partial y^{2}}+I_{13}^{*} \phi_{0}+L_{13}^{*} \psi_{0}-\frac{1}{2}\left(\frac{\partial w}{\partial x}\right)^{2}.
\end{aligned}
\tag{21}
$$

Introducing Eq (19) into Eq. (21) and substituting the resulting expression into Eq. (18) yields

$$
\begin{aligned}
&N_{x0}=g_{1} W+g_{2}\left(\mathrm{W}+2 \mu h\right) \mathrm{W}+g_{3} \phi_{0}+g_{4} \psi_{0}, \\
&N_{y0}=f_{1} W+f_{2}\left(\mathrm{W}+2 \mu h\right) \mathrm{W}+f_{3} \phi_{0}+f_{4} \psi_{0},
\end{aligned}
\tag{22}
$$

where g_i, $f_j\left(i, j=1 \div 5\right)$ are shown in Appendix.

Assuming a uniformly distributed transverse load with the form of $q=st$, the resulting equations are employed to investigate the nonlinear vibration of a microplate can be shown:

$$
\begin{aligned}
&W_{,tt}+o_{11} W+o_{11}^{*}\left(W+\mu h\right)+o_{12} W\left(W+\mu h\right)+o_{15} \phi+o_{16} \psi \\
&+o_{13}^{*}\left(W+\mu h\right)\left(W+2 \mu h\right)++o_{14} W\left(W+\mu h\right)\left(W+2 \mu h\right) \\
&+o_{13} W\left(W+2 \mu h\right)+o_{15}^{*} \phi\left(W+\mu h\right)+o_{16}^{*} \psi\left(W+\mu h\right)=n_{5} q, \\
&h_{41} \mathrm{W}+h_{42} \phi+h_{43} \psi=0, \\
&h_{51} \mathrm{W}+h_{43} \phi+h_{52} \psi=0.
\end{aligned}
\tag{23}
$$

in which $o_{1l}\left(l=1 \div 6\right), o_{1k}^{*}\left(k=1,3,5,6\right)$ are expressed in Appendix.

The fundamental frequency of nonlinear vibration of the microplate can be by finding the minimum value of the three solutions of the equation:

$$
\begin{vmatrix}
o_{11}+o_{11}^{*}-\omega^{2} & o_{15} & o_{16} \\
h_{41} & h_{42} & h_{43} \\
h_{51} & h_{43} & h_{52}
\end{vmatrix}=0
\tag{24}
$$

3. Results and Discussion

To assess the accuracy of the calculations, a comparison of the dimensionless natural frequency parameter $\omega=\frac{\omega a^{2}}{h} \sqrt{\frac{\rho_b}{C_{b11}}}$ with Monaco et al., [16], Ramirez et al., [17] and Ismail et al., [18]. Here, $\rho_b=5300\, kg/m^3$ and $C_{b11}=166 GPa$ are the bottom material's mass density and elasticity modulus

($BaTiO_3$). The plate is made of $BaTiO_3/CoFe_2O_4$ with $a = 2m, b = 1m$, and ratio $h/a = 0.2$. Based on the data presented in Table 1, it can be observed that the results obtained in this study are in excellent agreement with the previously published data.

Table 1. Comparison of the dimensionless frequencies $\bar{\omega}$ of an FG simply supported rectangular plate consisting of BaTiO3/CoFe2O4

Mode	Monaco et al., [16]	Ramirez et al., [17]	Ismail et al., [18]	This work
(1,1)	9.53	10.02	16.64	12.86
(2,2)	28.76	32.57	51.97	51.31

The geometrical parameters of the microplates chosen $h = 1\mu m, e_0 = 0.1, b/h = 80, \phi_0 = 50mV, \psi_0 = 20mA, V_{Batio3} = 50\%$. The following results evaluate how the dynamic response and natural frequency of microplates are influenced by geometrical and material parameters, as well as electric and magnetic potentials under uniformly distributed transverse load. Table 2 provides the material coefficients used in the study.

Table 2. The magnetic, piezo, electro properties of CoFe2O4 and BaTiO3

Notation	$C_{11}^f = C_{22}^f$	C_{12}^f	$C_{13}^f = C_{23}^f$	C_{33}^f	e_{31}^f	e_{33}^f	$\eta_{11}^f = \eta_{22}^f$	η_{33}^f
Unit	(GPa)				(C/m^2)		$(10^{-9} C/\mathrm{N}m^2)$	
CoFe2O4	286	173	170	269.5	0	0	0.08	1.2
Batio3	166	77	78	162	-4.4	18.6	0.093	12.6
Notation	$\mu_{11}^f = \mu_{22}^f$	μ_{33}^f	q_{31}^f	q_{33}^f	$m_{11}^f = m_{22}^f$	m_{33}^f	p_3^f	ρ_f
Unit	$(10^{-4}\ \mathrm{Ns}^2/\mathrm{C}^2)$		$(N/\mathrm{A}m)$		$(10^{-12}\ \mathrm{Ns/\ VC})$		$(10^{-7} C/m^2 K)$	(kg/m^3)
CoFe2O4	-5.9	1.57	580	700	0	0	0	5300
Batio3	0.05	0.1	0	0	0	0	0	5800

Table 3 respectively illustrates the impacts of applied electric and magnetic potentials on the natural frequencies of FG-MEE microplate. The natural frequency is observed to vary slightly with changes in the electric and magnetic potentials. An increase in electric potential leads to a rise in the natural frequency, while a decrease in magnetic potential results in a decline in the natural frequency. This trend can be attributed to a reduction in structural stiffness as the electric potential increases or the magnetic potential decreases, leading to a lower natural frequency.

Table 3. Variation of the natural frequencies $\left(\times 10^3\ s^{-1}\right)$ of the MEE plate depending on electric potential $\phi_0\,(mV)$, magnetic potential $\psi_0\,(mA)$

ϕ_0 \ ψ_0	-20	0	20
-50	4114.7853	4554.2702	4954.9265
0	4056.8218	4501.9687	4906.8973
50	3998.018	4449.0524	4858.3934

Table 4 provides insights into how the natural frequency of the FG-MEE microplate is effected by the width-to-thickness ratio and non-local parameters. An evident reduction in the natural frequency is observed as the b/h ratio is increased. This can be attributed to the larger plate resulting from the increase in the b/h ratio while keeping the thickness constant, leading to a lower load-carrying capacity. Furthermore, the nonlocal parameter have minimal influence on the frequency of FG-MEE micro-plate.

Table 4. Variation of the natural frequencies $\left(\times 10^3\ s^{-1}\right)$ of the MEE plate depending on ratio width to thickness b/h and nonlocal parameters e_0

b/h \ e_0	0	1	2
70	6239.6636	6239.6633	6239.6588
80	4858.3937	4858.3934	4858.3888
90	3910.1284	3910.1281	3910.1234

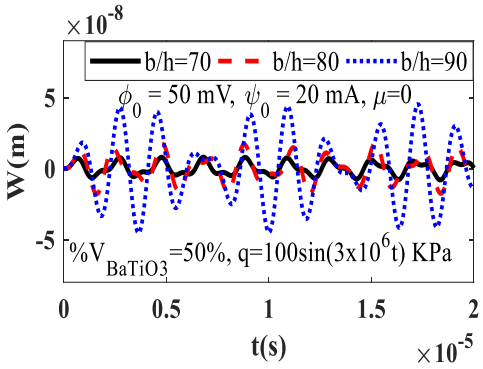

Figure 2. Change of ratio width-to-thickness *b/h* on the deflection.

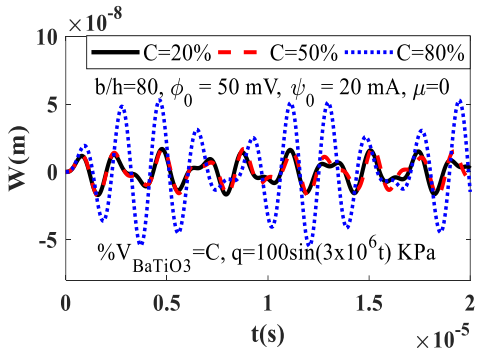

Figure 3. Change of volume fraction of piezoelectric phase on the deflection.

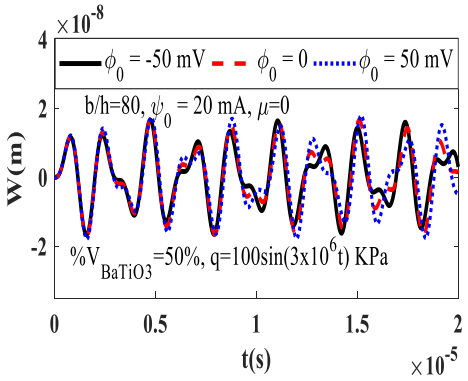

Figure 4. Change of electric potential on the deflection.

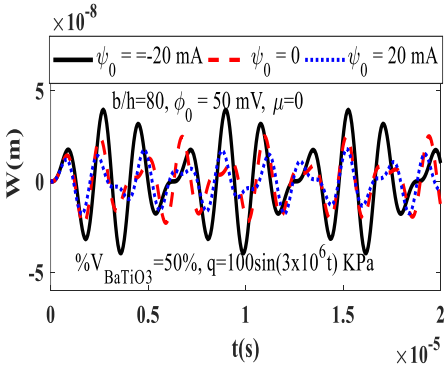

Figure 5. Change of magnetic potential on the deflection.

The behavior of MEE microplates with $h = 1\mu m, e_0 = 0.1$ is affected by various geometric parameters, including the width-to-thickness ratio b/h and volume fraction of piezoelectric phase

$V_{BatuiO3}$ can be observed in Fig. 2 and 3. It is evident from the figures that the deflection amplitude of the MEE plate increases significantly as the width-to-thickness b/h ratio or volume fraction of the piezoelectric phase $V_{BatuiO3}$ increases.

Fig. 4 and 5 respectively depict the variation of the nonlinear vibration of the MEE microplate with respect to the magnetic potential and electric potentials. The results presented in these figures demonstrate the opposite effect of magnetic and electric potentials on the deflection amplitude of the microplate. Increasing the magnetic potential from to leads to a reduction in the maximum deflection amplitude from -20 mA to 20 mA. In contrast, the change in maximum deflection amplitude due to the electric potential is negligible. Increasing the electric potential from -50 mV to 50 mV results in an increase of only 1% in the maximum deflection amplitude.

The influence of excitation force amplitude on the deflection amplitude curve of the FG-MEE microplates are depicted in Fig. 6. As indicated by the effect of the load has a marked effect on the deflection of the microplate. Obviously, as we increase the load, the deflection of the structure increases. Fig. 7 shows the effect of initial imperfection on the nonlinear vibration of the FG-MEE microplates, where the imperfection coefficient is denoted by $(\mu = 0, 0.1, 0.2)$. It can be observed that the imperfection coefficient has a considerable influence on the nonlinear vibration of the FG-MEE microplates.

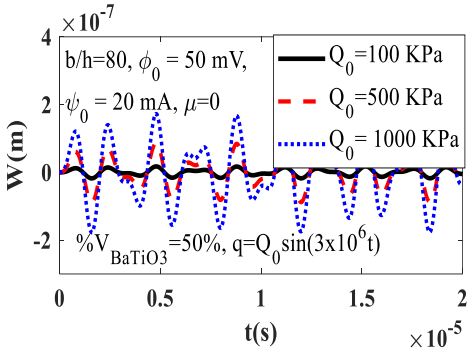

Figure 6. Change of excitation force amplitude on the deflection.

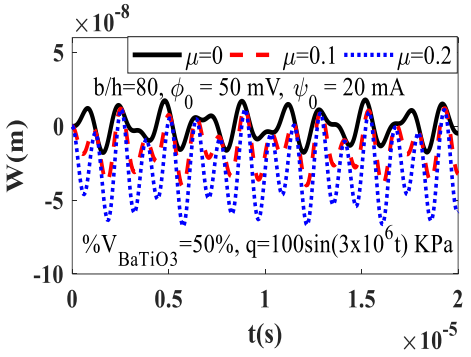

Figure 7. Change of imperfect coefficients on the deflection.

4. Conclusion

In this work the nonlinear vibration of FG-MEE microplates under mechanic-magneto-electro loads based on a nonlocal stress theory were studied. From obtained reults, following conclusions can be given:

- The natural frequency decreases with increasing electric potential or decreasing magnetic potential.

- The volume fraction of the piezoelectric phase has a negative impact on the nonlinear vibration of the microplate.

- Increasing the initial imperfection parameter results in a notable decrease in the deflection amplitude.

- The vibration characteristics of the microplate are highly dependent on its geometrical parameters.

Acknowledgments

This work has been supported/partly supported by VNU University of Engineering and Technology under project number CN22.17. Ngo Dinh Dat was funded by the Master, PhD Scholarship Programme of Vingroup Innovation Foundation (VINIF), VINIF.2022.TS021. The authors are grateful for this support.

References

[1] D. Young, C. Zorman, M. Mehregany, MEMS/NEMS Devices and Applications, In: Springer handbook of Nanotechnology, Springer Handbooks, 2007, pp. 415-42, https://doi.org/10.1007/978-3-540-29857-1_15.

[2] L. Zhou, M. Li , W. Tian, P. Liu, Coupled Multi-Physical Cell-Based Smoothed Finite Element Method for Static Analysis of Functionally Grade Magneto-Electro-Elastic Structures at Uniform Temperature, Composite Structures, Vol. 226, 2019, pp. 111238, https://doi.org/10.1016/j.compstruct.2019.111238.

[3] L. Zhou, M. Li, Y. Cai, H. Zhao, E. Zhao, The Multi-Physic Cell-Based Smoothed Finite Element Method for Dynamic Characterization of Magneto-Electro-Elastic Structures under Thermal Conditions, Composite Structures, Vol. 240, 2020, pp. 112045, https://doi.org/10.1016/j.compstruct.2020.112045.

[4] C. Hsu, C. Hwu, Coupled Stretching-Bending Boundary Element Analysis for Unsymmetric Magneto-Electro-Elastic Laminates with Multiple Holes, Cracks and Inclusions, Engineering Analysis with Boundary Elements, Vol. 139, 2022, pp. 137-151, https://doi.org/10.1016/j.enganabound.2022.03.018.

[5] H. Kuo, Y. Wang, Wave Motion of Magneto-Electro-Elastic Laminated Plates Withmembrane-Type Interfacial Imperfections, Composite Structures, Vol. 293, 2022, pp. 115661, https://doi.org/10.1016/j.compstruct.2022.115661.

[6] X. Zhang, Q. Xu, X. Zhao, Y. Li, J. Yang, Nonlinear Analyses of Magneto-Electro-Elastic Laminated Beams in Thermal Environments, Composite Structures, Vol. 234, 2020, pp. 111524, https://doi.org/10.1016/j.compstruct.2019.111524.

[7] M. Vinyas, K. Sunny, D. Harursampath, N. T. Trung, M. Loja, Influence of Interphase on the Multi-Physics Coupled Frequency of Three-Phase Smart Magneto-Electro-Elastic Composite Plates, Composite Structures, Vol. 226, 2019, pp. 111254, https://doi.org/10.1016/j.compstruct.2019.111254.

[8] L. Zhou, M. Li, Y. Cai, H. Zhao, E. Zhao, The Multi-Physic Cell-Based Smoothed Finite Element Method for Dynamic Characterization of Magneto-Electro-Elastic Structuresu Thermal Conditions, Composite Structures, Vol. 240, 2020, pp. 112045, https://doi.org/10.1016/j.compstruct.2020.112045.

[9] J. Chen, H. Chen, E. Pan, P. R. Heyliger, Modal Analysis of Magneto-Electro-Elastic Plates using the State-Vector Approach, Journal of Sound and Vibration, Vol. 304, 2007, pp. 722-34, https://doi.org/10.1016/j.jsv.2007.03.021.

[10] N. D. Dat, T. Q. Quan, M. Vinyas, N. D. Duc, Analytical Solutions for Nonlinear Magneto-Electro-Elastic Vibration of Smart Sandwich Plate with Carbon Nanotube Reinforced Nanocomposite Core in Hygrothermal Environment, International Journal of Mechanical Sciences, Vol. 186, 2020, pp. 105906, https://doi.org/10.1016/j.ijmecsci.2020.105906.

[11] N. D. Dat, T. Q. Quan, N. D. Duc, Vibration Analysis of Auxetic Laminated Plate with Magneto-Electro-Elastic Face Sheets Subjected to Blast Loading, Composite Structures, Vol. 280, 2022, pp. 114925, http://dx.doi.org/10.1016/j.compstruct.2021.114925.

[12] H. T. Liu, Y. H. Qie, Y. G. Zhou, Investigation of Non-Local Theory Solution to A Three-Dimensional Rectangular Permeable Crack in Magneto-Electro-Elastic Materials, International Journal of Mechanical Sciences, Vol. 134, 2017, pp. 460-78, https://doi.org/10.1016/j.ijmecsci.2017.10.039.

[13] L. L. Zhang, J. X. Liu, X. Q. Fang, G. Q. Nie, Effects of Surface Piezoelectricity and Nonlocal Scale on Wave Propagation in Piezoelectric Nanoplates, European Journal of Mechanics A/Solids, Vol. 46, 2014, pp. 22-29, http://dx.doi.org/10.1016/j.euromechsol.2014.01.005.

[14] J. Y. Chen, J. H. Guo, E. N. Pan, Reflection and Transmission of Plane Wave in Multilayered Nonlocal Magneto-Electro-Elastic Plates Immersed in Liquid, Composite Structures, Vol. 162, 2017, pp. 401-410, http://dx.doi.org/10.1016/j.compstruct.2016.11.004.

[15] S. Sahmani, M. M. Aghdam, T. Rabczuk, Nonlocal Strain Gradient Plate Model for Nonlinear Large-Amplitude Vibrations of Functionally Graded Porous Micro/Nano-Plates Reinforced with GPLs, Composite structures, Vol. 198, 2018, pp. 51-62, https://doi.org/10.1016/j.compstruct.2018.05.031.

[16] G. Monaco, N. Fantuzzi, F. Fabbrocino, R. Luciano, Critical Temperatures for Vibrations and Buckling of Magneto-Electro-Elastic Nonlocal Strain Gradient Plates, Nanomaterials, Vol. 11, No. 1, 2021, pp. 1-18, https://doi.org/10.3390/nano11010087.

[17] F. Ramirez, P. Heyliger, E. Pan, Discrete Layer Solution to Free Vibrations of Functionally Graded Magneto-Electro-Elastic Plates, Mechanics of Advanced Materials and Structures, Vol. 13, No. 3, 2006, pp. 249-66, http://dx.doi.org/10.1080/15376490600582750.

[18] E. Ismail, O. Ramazan, Thermal Vibration and Buckling of Magneto-Electro-Elastic Functionally Graded Porous Nanoplates using Nonlocal Strain Gradient Elasticity, Composite structures, Vol. 296, 2022, pp. 115878, https://doi.org/10.1016/j.compstruct.2022.115878.

Appendix

$$\left(I_{ij},\, L_{ij},\, K_{ij}\right)=\int_{\frac{-h}{2}}^{\frac{h}{2}}\overline{C_{ij}}(1,\, z,z^2)\,dz, ij=11,12,22,66, \left(I_{13},I_{23}\right)=\int_{\frac{-h}{2}}^{\frac{h}{2}}\overline{e_{31}}\left(1,z\right)dz,\ \left(I_{14},I_{24}\right)=\int_{\frac{-h}{2}}^{\frac{h}{2}}\overline{e_{32}}\left(1,z\right)dz,$$

$$\left(L_{13},L_{23}\right)=\int_{\frac{-h}{2}}^{\frac{h}{2}}\overline{q_{31}}\left(1,z\right)dz, \left(L_{14},L_{24}\right)=\int_{\frac{-h}{2}}^{\frac{h}{2}}\overline{q_{32}}\left(1,z\right)dz, \mathrm{i}=1,3;\ j=2,4.$$

$$y_{11}=-\left[X_{11}^{*}\lambda_m^4+X_{22}^{*}\delta_n^4+\left(X_{12}^{*}+X_{21}^{*}+4X_{66}^{*}\right)\lambda_m^2\delta_n^2+k_1+k_2\left(\lambda_m^2+\delta_n^2\right)\right]+$$

$$\left[\begin{matrix}L_{21}^{*}\left(\lambda_m^4-\eta\left(\lambda_m^6+\lambda_m^4\delta_n^2\right)\right)+L_{12}^{*}\left(\delta_n^4-\eta\left(\delta_n^6+\lambda_m^2\delta_n^4\right)\right)\\+\left(L_{11}^{*}+L_{22}^{*}-2L_{66}^{*}\right)\left(\lambda_m^2\delta_n^2-\eta\left(\lambda_m^2\delta_n^4+\lambda_m^4\delta_n^2\right)\right)\end{matrix}\right]Y_3,\ y_{12}=-\frac{32\lambda_m\delta_n}{3ab}Y_3,$$

$$y_{13}=-\frac{8\lambda_m\delta_n}{3ab}\left(\frac{L_{21}^{*}}{I_{11}^{*}}+\frac{L_{12}^{*}}{I_{22}^{*}}\right), y_{14}=-\frac{1}{16}\left(\frac{\lambda_m^4}{I_{22}^{*}\left(4\eta\delta_n^2+1\right)}+\frac{\delta_n^4}{I_{11}^{*}\left(4\eta\lambda_m^2+1\right)}\right), y_{15}=X_{31}^{*}\lambda_m^2+X_{32}^{*}\delta_n^2,$$

$$y_{16}=X_{41}^{*}\lambda_m^2+X_{42}^{*}\delta_n^2, y_{41}=-\left(Q_{11}\lambda_m^2+T_{12}\delta_n^2\right), y_{42}=-\left(Q_{13}\lambda_m^2+Q_{14}\delta_n^2-n_{33}^{*}\right)$$

$$y_{43}=-\left(Q_{15}\lambda_m^2+Q_{16}\delta_n^2-m_{33}^{*}\right), y_{51}=-\left(Q_{21}\lambda_m^2+Q_{22}\delta_n^2\right), y_{52}=-\left(Q_{23}\lambda_m^2+Q_{24}\delta_n^2-\mu_{33}^{*}\right)$$

$$g_1=-\frac{\left(\left(I_{11}^{*}L_{11}^{*}+I_{12}^{*}L_{21}^{*}\right)\lambda_m^2+\left(I_{11}^{*}L_{12}^{*}+I_{12}^{*}L_{22}^{*}+M_3\left(I_{11}^{*}I_{22}^{*}-I_{12}^{*\,2}\right)\right)\delta_n^2\right)}{ab\left(I_{12}^{*\,2}-I_{11}^{*}I_{22}^{*}\right)}\frac{4}{\lambda_m\delta_n}+\frac{4\delta_n}{ab\lambda_m}M_3\eta\left(\lambda_m^2+\delta_n^2\right),$$

$$g_2=-\frac{I_{11}^{*}\lambda_m^2+I_{12}^{*}\delta_n^2}{8\left(I_{12}^{*\,2}-I_{11}^{*}I_{22}^{*}\right)}, g_3=\frac{I_{11}^{*}I_{13}^{*}+I_{12}^{*}I_{14}^{*}}{\left(I_{12}^{*\,2}-I_{11}^{*}I_{22}^{*}\right)}, g_4=\frac{I_{11}^{*}L_{13}^{*}+I_{12}^{*}L_{14}^{*}}{\left(I_{12}^{*\,2}-I_{11}^{*}I_{22}^{*}\right)},$$

$$f_1=-\frac{\left(\left(I_{12}^{*}L_{11}^{*}+I_{22}^{*}L_{21}^{*}+M_3\left(I_{11}^{*}I_{22}^{*}-I_{12}^{*\,2}\right)\right)\lambda_m^2+\left(I_{12}^{*}L_{12}^{*}+I_{22}^{*}L_{22}^{*}\right)\delta_n^2\right)}{ab\left(I_{12}^{*\,2}-I_{11}^{*}I_{22}^{*}\right)}\frac{4}{\lambda_m\delta_n}+\frac{4\lambda_m}{ab\delta_n}M_3\eta\left(\lambda_m^2+\delta_n^2\right),$$

$$f_2=-\frac{I_{12}^{*}\lambda_m^2+I_{22}^{*}\delta_n^2}{8\left(I_{12}^{*\,2}-I_{11}^{*}I_{22}^{*}\right)}, f_3=\frac{I_{12}^{*}I_{13}^{*}+I_{22}^{*}I_{14}^{*}}{\left(I_{12}^{*\,2}-I_{11}^{*}I_{22}^{*}\right)}, f_4=\frac{I_{12}^{*}L_{13}^{*}+I_{22}^{*}L_{14}^{*}}{\left(I_{12}^{*\,2}-I_{11}^{*}I_{22}^{*}\right)}.$$

$$X_{11}^{*}=K_{11}-L_{11}^{*}L_{11}-L_{21}^{*}L_{12},X_{22}^{*}=K_{22}-L_{12}^{*}L_{12}-L_{22}^{*}L_{22},X_{12}^{*}=K_{12}-L_{12}^{*}L_{11}-L_{22}^{*}L_{12},$$
$$X_{21}^{*}=K_{12}-L_{11}^{*}L_{12}-L_{21}^{*}L_{22},\ X_{66}^{*}=K_{66}-L_{66}^{*}L_{66},X_{31}^{*}=\left(-I_{23}\right)\beta\sin\left(\beta z\right),X_{32}^{*}=\left(-I_{24}\right)\beta\sin\left(\beta z\right),$$
$$X_{41}^{*}=\left(-L_{23}\right)\beta\sin\left(\beta z\right),X_{42}^{*}=\left(-L_{24}\right)\beta\sin\left(\beta z\right),\mu_{33}^{*}=-\int_{\frac{-h}{2}}^{\frac{h}{2}}\mu_{33}\left(\beta\sin\left(\beta z\right)\right)^{2}dz$$
$$Q_{13}=\int_{\frac{-h}{2}}^{\frac{h}{2}}\eta_{11}\cos^{2}\left(\beta z\right)dz,Q_{15}=\int_{\frac{-h}{2}}^{\frac{h}{2}}m_{11}\cos^{2}\left(\beta z\right)dz,Q_{14}=\int_{\frac{-h}{2}}^{\frac{h}{2}}\eta_{22}\cos^{2}\left(\beta z\right)dz$$
$$Q_{16}=\int_{\frac{-h}{2}}^{\frac{h}{2}}m_{22}\cos^{2}\left(\beta z\right)dz\ ,Q_{11}=-\int_{\frac{-h}{2}}^{\frac{h}{2}}e_{31}z\beta\sin\left(\beta z\right)dz,Q_{12}=-\int_{\frac{-h}{2}}^{\frac{h}{2}}e_{32}z\beta\sin\left(\beta z\right)dz$$
$$\eta_{33}^{*}=-\int_{\frac{-h}{2}}^{\frac{h}{2}}\eta_{33}\left(\beta\sin\left(\beta z\right)\right)^{2}dz,m_{33}^{*}=-\int_{\frac{-h}{2}}^{\frac{h}{2}}m_{33}\left(\beta\sin\left(\beta z\right)\right)^{2}dz,Q_{23}=\int_{\frac{-h}{2}}^{\frac{h}{2}}\mu_{11}\cos^{2}\left(\beta z\right)dz$$
$$Q_{24}=\int_{\frac{-h}{2}}^{\frac{h}{2}}\mu_{22}\cos^{2}\left(\beta z\right)dz,Q_{21}=-\int_{\frac{-h}{2}}^{\frac{h}{2}}q_{31}z\beta\sin\left(\beta z\right)dz,Q_{22}=-\int_{\frac{-h}{2}}^{\frac{h}{2}}q_{32}z\beta\sin\left(\beta z\right)dz$$